Study by EXAFS, Raman, and NMR Spectroscopies of the Genesis of Oxidic Precursors of Zeolite-Supported HDS Catalysts

Guillaume Plazenet,[†,‡,§] Edmond Payen,*[,†] John Lynch,[‡,||] and Bernadette Rebours[‡,⊥]

Laboratoire de Catalyse de Lille, UPRESA CNRS 8010, Université des Sciences et Technologies de Lille, Bât. C3, 59655 Villeneuve d'Ascq Cedex, France, and Institut Français du Pétrole,1 et 4, Avenue de Bois-Préau, 92852 Rueil-Malmaison Cedex, France

Received: February 26, 2002

A 3 wt % Mo zeolite-supported oxidic precursor prepared from ammonium heptamolybdate by incipient wetness impregnation was studied using Raman and ^{27}Al NMR spectroscopies, at the various steps of its preparation. The formation of an Anderson type aluminomolybdate anion, which was preserved during drying, was observed. This species led to the formation of aluminum molybdate $Al_2(MoO_4)_3$ upon calcination and was partially reformed upon rehydration of the sample. XANES and EXAFS experiments at the Mo K-edge confirmed these results and showed the Anderson entity to be the majority species. The use of different loadings and supports showed that the Anderson entity is formed through extraction from the zeolite of nonframework aluminum atoms and that ammonium heptamolybdate precipitates when the Mo loading is too high. EXAFS and XRD experiments applied to another sample prepared by MoO_3 vapocondensation showed that the observed Anderson entity cannot be situated in the supercages of the zeolite.

Introduction

With increasing social awareness of environmental risks, the will to reduce toxic emissions has increased, and the quality of the fuels becomes a key factor. In particular, the legislation concerning the quantity of sulfur emission is increasingly severe, and limits are expected to go down to 50 ppm in the years to come. This imposes improvements in catalytic hydrotreatment (HDT) of the petroleum feedstocks in general and in hydrodesulfurization (HDS) in particular. Catalyst improvement requires a better understanding of the structure and genesis of the active phases consisting of well dispersed molybdenum disulfide on a high specific surface area support. These nanocrystallites are generally promoted by cobalt or nickel atoms. The active phases are obtained through the sulfidation of an oxidic precursor generally prepared by impregnation of the support with an aqueous solution of the elements to be deposited.

Numerous studies over many years have concerned the structure of the active phases of these catalysts, the study of which is necessary to improve their performances. Concurrently, many articles have been published that deal with the oxidic phases, which, as precursors, are key to catalyst preparation. If one wants to create more active catalysts, one has first to know the way the current ones function and are formed.

In the case of the most common support, i.e., alumina, it has been thought for a long time that the entities present in the impregnating solution remain intact upon adsorption on the alumina surface. Thus it was generally admitted that isolated tetrahedral and adsorbed heptamolybdate entities were respectively present at low and intermediate Mo loading, whereas bulk MoO_3 was identified at higher Mo loadings after the completion of the monolayer as defined by XPS[1−4]. However the existence of a "hydrate" form of an aluminum molybdate at the surface of the alumina has also been suggested, whereas the formation of an aluminum heteropolymolybdate was previously argued by Goncharova et al.[5] or Spozhakina et al.[6] More recently, Carrier et al.[7−11] showed that some aluminum atoms of the support are extracted during the equilibrium impregnation to give the aluminomolybdate ion $AlMo_6O_{24}H_6^{3-}$ ($AlMo_6$), whereas a Raman spectroscopic study[12,13] of the oxomolybdate surface phase of a Mo/Al_2O_3 prepared by incipient wetness impregnation revealed the presence of well dispersed aluminomolybdate entities interacting with the support, these entities being preserved during the drying step. Moreover it has been shown that the nature of the surface oxomolybdate phase after calcination is dependent on its degree of hydration, a remark that leads to considering the necessity of in situ characterization of the oxidic precursor.

Zeolites are an alternative support, which are increasingly studied, because their acid properties are very appreciated in catalytic cracking. It is widely known that zeolites contain, in addition to framework aluminum, variable amounts (depending on the nature of the zeolite and the treatments it has been submitted to) of amorphous alumina and Al^{3+} ions, which may also react to give the aluminomolybdate entity upon impregnation with ammonium heptamolybdate (AHM) solutions. Consequently, it is of greatest interest to see whether the same dissolution−precipitation phenomenon can be transferred from alumina-supported to zeolite-supported systems.

Many spectroscopic techniques, such as NMR and Raman spectroscopies, have been used to characterize the structure of these precursors but alone they do not clarify the exact nature of the oxidic phase precursor of the HDS active phase. EXAFS and XANES are nowadays among the most powerful methods of local order characterization in highly dispersed metal catalysts.[14,15] This method is especially useful for investigation

* To whom correspondence should be addressed. Phone: 33.3.20.43.49.47. Fax: 33.3.20.43.65.61. E-mail: Edmond.Payen@univ-lille1.fr.
† Université des Sciences et Technologies de Lille.
‡ Institut Français du Pétrole.
§ E-mail: Guillaume.Plazenet@univ-lille1.fr. Fax: 33.3.20.49.65.61.
|| E-mail: john.lynch@ifp.fr. Fax: 33.1.47.52.70.57.
⊥ E-mail: bernadette.rebours@ifp.fr. Fax: 33.1.47.52.70.57.

10.1021/jp020538m CCC: $22.00
Published on Web 06/21/2002

of the environment of amorphous phases and small metal particles, which are very difficult to study by other techniques. In many cases, information can be gathered (in situ) during the processes of preparation, when the catalyst is inaccessible to for example traditional surface analysis. Although EXAFS appears as an ideal tool for such studies, previous EXAFS studies were mainly devoted to $CoMo/Al_2O_3$ catalysts for the determination of the local Co environment. Some authors discussed the Mo structures, but the results were interpreted without taking into account the possible existence of the aforementioned heteropolymolybdenum species.

The objective of this work is to combine NMR, Raman spectroscopy, and EXAFS to determine the local structure of the precursor of the MoS_2/Zeolite HDS active phase. In a first part, this work will analyze the species present on Faujasitic-type HY zeolite after its impregnation with an ammonium heptamolybdate (AHM) solution, and their evolution during the preparation. We will show that the Anderson entity formerly detected on the alumina can also be found here. Second, we will determine the process of formation of this entity, i.e., the origin of the aluminum atoms. Finally, we will present an attempt to localize the aluminomolybdate anion on/in the support.

Experimental Section

Catalysts Preparation. All of the products used in the preparations were certified pure reagent grade from Fluka and were used without further purification. The reference samples $Al_2(MoO_4)_3$ and aluminomolybdate ammonium salt were respectively supplied by Alfa Aesar and prepared according to the method described by Hall.[16] The structure of $Al_2(MoO_4)_3$ was checked by X-ray diffraction (JCPDS[17] n°20−0034). Most of the samples were prepared by incipient wetness impregnation. An aqueous solution of AHM was prepared, with its concentration depending on the desired Mo loading (57 g/L for 3 wt %). The zeolite was impregnated with the appropriate volume of solution. During the following maturation step, the samples were left in ambient air for 2 h. These are called the "matured" samples. The samples were then dried at 100 °C overnight, to give what we call the "dried" samples. Then there was the calcination step, at 500 °C for 4 h after a temperature increase of 50 °C/h. After cooling, the samples were submitted to the rehydration step, by placing them in a closed water-saturated atmosphere for 48 h. This step was aimed at evaluating the effect of the atmosphere on the calcined sample and gave the samples called "rehydrated".

The other way of preparation considered here is MoO_3 vapocondensation. Stoechiometric quantities of MoO_3 and zeolite (to get a loading of 2 wt % in molybdenum) were crushed and intimately mixed together and introduced in a quartz reactor. The mixture was heated at 100 °C for 1 h and then at 700 °C for 1 h, after a temperature increase of 50 °C/h, under a very low N_2 flow. This sample was only studied in its final calcined state.

Nomenclature. The nomenclature used in this paper consists of one number and two letters separated by a slash. The number represents the Mo loading in weight percent of the sample, the first letter the state of the sample (M for matured, D for dried, C for calcined, R for rehydrated, and V for the samples obtained by MoO_3 vapocondensation) and the second letter the support, since three types of zeolites are used. Bulk Si/Al ratios were determined by X-ray fluorescence, framework Si/Al ratios by ^{29}Si NMR, and porous volumes by incipient wetness impregnation of water. The main features are described in Table 1 (name, applied treatments, characteristics). For instance, 3D/E represents the 3 Mo wt % sample in the dried state, supported on the EDTA-treated zeolite. The zeolite called W, that was steamed and then acid washed, is the one most completely studied in this paper, the two other zeolites being used to draw comparisons.

TABLE 1: Characteristics of the Various Zeolites Used in This Study

name	treatments	$(Si/Al)_{structure}$	$(Si/Al)_{bulk}$	porous volume (mL/g)
S	steamed	19	2.8	1.04
W	steamed and acid washed	19	13.6	1.00
E	steamed, EDTA-treated, and NH_4NO_3 exchanged	10	10	1.00

Physical Measurements. *Raman Measurements.* The Raman spectra of the samples, maintained at room temperature, were recorded using a Raman microprobe (Infinity from Dilor), equipped with a photodiode array detector. The exciting light source was the 532 nm line of a Nd:YAG laser, and the wavenumber accuracy was 2 cm^{-1}.

NMR Measurements. ^{27}Al NMR measurements of the samples were carried out on a Bruker AC400 spectrometer, calibrated with a 1 M solution of aluminum nitrate. Liquid NMR spectra were recorded for the matured and rehydrated samples, to analyze the entities in aqueous solution within the pores of the support, whereas magic angle spinning (MAS) was used for the dried and calcined samples. Using transfer in a glovebox under N_2 atmosphere, the calcined samples have gone through an "in situ like" analysis and been preserved from the water present in ambient air.

XAS Measurements. The experiments were carried out in the Laboratoire pour l'Utilisation du Rayonnement Electromagnétique (Orsay) at the EXAFS D42 and D44 beamlines using synchrotron radiation from the DCI storage ring running at 1.85 GeV with an average current of 250 mA. The XAS data were taken in the transmission mode through a double crystal monochromator (Ge(400) for the Mo K-edge and Si(111) for the Mo L-edge) using two ion chambers as detectors. The analysis time for an X-ray absorption spectrum (19900−20900 eV) was about 15 min, and three spectra were recorded for each sample. The spectra of reference products were also recorded: ammonium heptamolybdate (referred to as AHM) in solid phase and in aqueous solution (430 g/L), aluminum Anderson salt (referred to as $AlMo_6$) in solid phase and in aqueous solution (25.6 g/L), and $Al_2(MoO_4)_3$ in solid phase. XAS of the calcined samples was recorded in situ. The dried catalyst was transferred into a treatment cell dedicated to in situ XAS experiments, which has been previously described.[16] It is composed of a sample holder connected to a gas rack that allows control of the atmosphere flowing through the sample. The sample holder is placed in a stainless steel heater, with two X-ray transparent windows. In the cell, the catalyst was calcined according to the experimental conditions described above, and the XAS spectrum was recorded at room temperature (RT).

The X-ray absorption near edge spectra were normalized with the first inflection point of the edge fixed at the theoretical value of the absorption edge (19.999 keV for the K-edge, 2.52 keV for the L-edge), and with the first inflection point of the first EXAFS oscillation fixed at an intensity of 1.

The Mo K-edge extended X-ray absorption fine structure regions of the spectra were extracted and analyzed using A.

Michalowicz's software packages EXAFS 98 ppc and Round Midnight.[17] The EXAFS spectrum was first transformed from k space (k^3, Kaiser window 3.6−15 $Å^{-1}$) to R space to obtain the radial distribution function (RDF). The EXAFS spectrum for one or several coordination shells was isolated by inverse Fourier transform of the RDF over the appropriate region (0.9−3.7 Å) and fitted using the single scattering EXAFS equation with amplitude and phase functions calculated by FEFF.[18−21]

XRD Measurements. XRD experiments were performed on a Philips PW1050 goniometer in Bragg−Brentano geometry with copper Kα radiation, a graphite secondary monochromator, and a sample spinner. Data were collected over a 2−72° 2θ range, with a 0.02° step size and a counting time of 3 s per step.

Results and Discussion

Genesis of the Oxidic Precursor. Figure 1 shows Raman spectra of 3M/W, 3D/W, 3C/W, and 3R/W, together with those of $AlMo_6$, $Al_2(MoO_4)_3$, and the bare zeolite. For the samples 3M/W and 3D/W (Figure 1a), the Raman spectra exhibit the characteristic lines of the zeolite at 507, 490, and 315 cm^{-1}. However, the broad line around 1100 cm^{-1}, attributed to the amorphous alumina,[22] is not seen for the Mo-loaded samples. These samples also exhibit the well-defined spectrum of the Anderson entity $AlMo_6$,[13] with the main lines being observed at 952 and 902 cm^{-1} (attributed to symmetric and antisymmetric stretching modes of the MoO_{2t} groups), at 575 cm^{-1} (attributed to the Al−O stretching mode), and at 390, 365, and 225 cm^{-1} (attributed to the deformation modes). In their work, Le Bihan et al.[13] found that the Raman spectrum of $AlMo_6$ in solution is slightly modified: the line at 575 cm^{-1} is shifted at 560 cm^{-1} and the shoulder between the two peaks at 902 and 952 cm^{-1} disappears. As these modifications are not seen in our case, we can deduce that the $AlMo_6$ entity detected on 3M/W is not in solution but in a precipitated form. Upon calcination (Figure 1b), the spectra are modified. The spectrum of 3C/W shows the lines of the zeolite at 507 and 490 cm^{-1} superimposed on the broad underlying lines of the glass in situ cell and a line at 1002 cm^{-1}, which indicates the presence of $Al_2(MoO_4)_3$ on the sample. Indeed, the line at 1002 cm^{-1} is assigned to the stretching mode of the $Mo-O_t$ bonds, and the bulk reference salt $Al_2(MoO_4)_3$ presents such bonds. However, the low spectra range features of $Al_2(MoO_4)_3$ are not observed, showing that the observed species do not present any long range order. The line at 980 cm^{-1} most likely corresponds to a polymolybdate phase, but it has not been ascribed to a specific structure. This line at 980 cm^{-1} is found again in 3R/W (Figure 1a), showing that this entity is not affected by the rehydration process. Moreover, $Al_2(MoO_4)_3$ is no longer observed, whereas the lines characteristic of $AlMo_6$ reappear at 952 and 902 cm^{-1} and also at 360 and 220 cm^{-1}.

These results suggest that we have the same kind of behavior as in alumina-supported samples: it seems that the impregnation of the HY zeolite with the AHM solution results in the formation of the aluminomolybdate anion, which is preserved in the drying phase and transformed into a "surface" aluminum molybdate during calcination, while an undefined polymolybdate phase appears. The latter is conserved upon rehydration, and $AlMo_6$ is recovered. However, although the Raman spectra of the matured and dried samples are unambiguous, the exact nature of the supported oxomolybdate phase obtained after calcination or after rehydration is not clearly established.

Figure 2 presents ^{27}Al NMR spectra in the solid and liquid states for the matured and rehydrated samples and in the solid state for the dried and calcined ones, together with those of $AlMo_6$ and $Al_2(MoO_4)_3$. The MAS NMR spectrum of the zeolite (Figure 2a) exhibits two peaks, one intense at 60 ppm and one weak at 0 ppm respectively assigned to the tetrahedral (framework) and octahedral (nonframework) Al atoms of the zeolite.[23] The 3M/W and 3D/W samples exhibit the peak at 60 ppm together with a peak at 15 ppm ascribed to the ammonium aluminomolybdate, but the peak at 0 ppm has disappeared. The ^{27}Al liquid-state NMR spectrum of sample 3M/W (Figure 2b), sensitive to the solution present in the pores of the support, also shows the main peak at 15 ppm characteristic of $AlMo_6$.

After calcination (Figure 2c), the peak at −14 ppm characteristic of $Al_2(MoO_4)_3$ is observed for 3C/W. In $Al_2(MoO_4)_3$, the aluminum atoms occupy four different sites,[24] but to differentiate them in NMR requires experiments based on satellite transitions,[25] not applied in this work. Here, the spectrum of the bulk reference exhibits two different peaks, at −12 and −14 ppm, as described in the literature,[26] indicating only two inequivalent aluminum sites. The observation of these two lines on a supported sample also requires specific NMR experiments. Because of dehydration effects, the two lines of the zeolite at 60 and 0 ppm are transformed to a very broad and poorly resolved peak. The zeolite shows a high crystalline field gradient; the presence of water homogenizes the field and so decreases the gradient, decreasing in the same time the range of quadrupolar shifts, and allowing the appearance of two peaks. Solid-state NMR on 3R/W (Figure 2a) shows the line at 15 ppm characteristic of $AlMo_6$, together with the peak at 0 ppm ascribed to dissolved aluminum atoms (very sharp because of hydration), that was not seen for samples 3M/W and 3D/W. This peak is also present on the liquid-state spectrum (Figure 2b), together with a peak at 15 ppm less intense than in 3M/W, more as a shoulder on the broad underlying Probe signal of the spectrometer at 65 ppm. This shows that upon impregnation all of the Al^{VI} species, characterized by the peak at 0 ppm, have been used to form $AlMo_6$, and only a fraction is liberated upon rehydration. This indicates that the reformation of $AlMo_6$ upon rehydration is not complete, as will be confirmed later.

NMR enables us to confirm the Raman results, giving supporting evidence of the presence of $AlMo_6$ in the zeolite-supported samples in the matured and dried states. They also prove that the calcination of the dried sample leads to an aluminum molybdate phase, which reverts partly to $AlMo_6$ during the rehydration. NMR has the advantage of being able to screen only the liquid phase: liquid-state NMR confirmed the presence of the Anderson entity in the aqueous solution captured in the pores of the support, together with its presence in a precipitated form as seen by Raman. This is also true for the Anderson entities restored upon rehydration. It seems likely that the quantity of water absorbed by the zeolite is insufficient and that the limit of solubility of $AlMo_6$ is reached.

However, even if they show the formation of $AlMo_6$ upon incipient wetness impregnation of the zeolite with an AHM solution, these results do not show if its formation is quantitative. Other isopolymolybdenum species, not visible by ^{27}Al NMR nor Raman spectroscopies, may exist. The liquid-state ^{95}Mo NMR spectrum of 3M/W (see Figure 3) exhibits a single peak at −20 ppm, characteristic, according to the literature, of $AlMo_6$.[7] This confirms the presence of $AlMo_6$ as the only Mo-containing phase on the matured sample. The concentration of the species in solution in the 3R/W sample was too low for them to be observed by liquid state ^{95}Mo NMR. Unfortunately, because of low sensitivity, no information is available concerning the presence or absence of other molybdenum species in

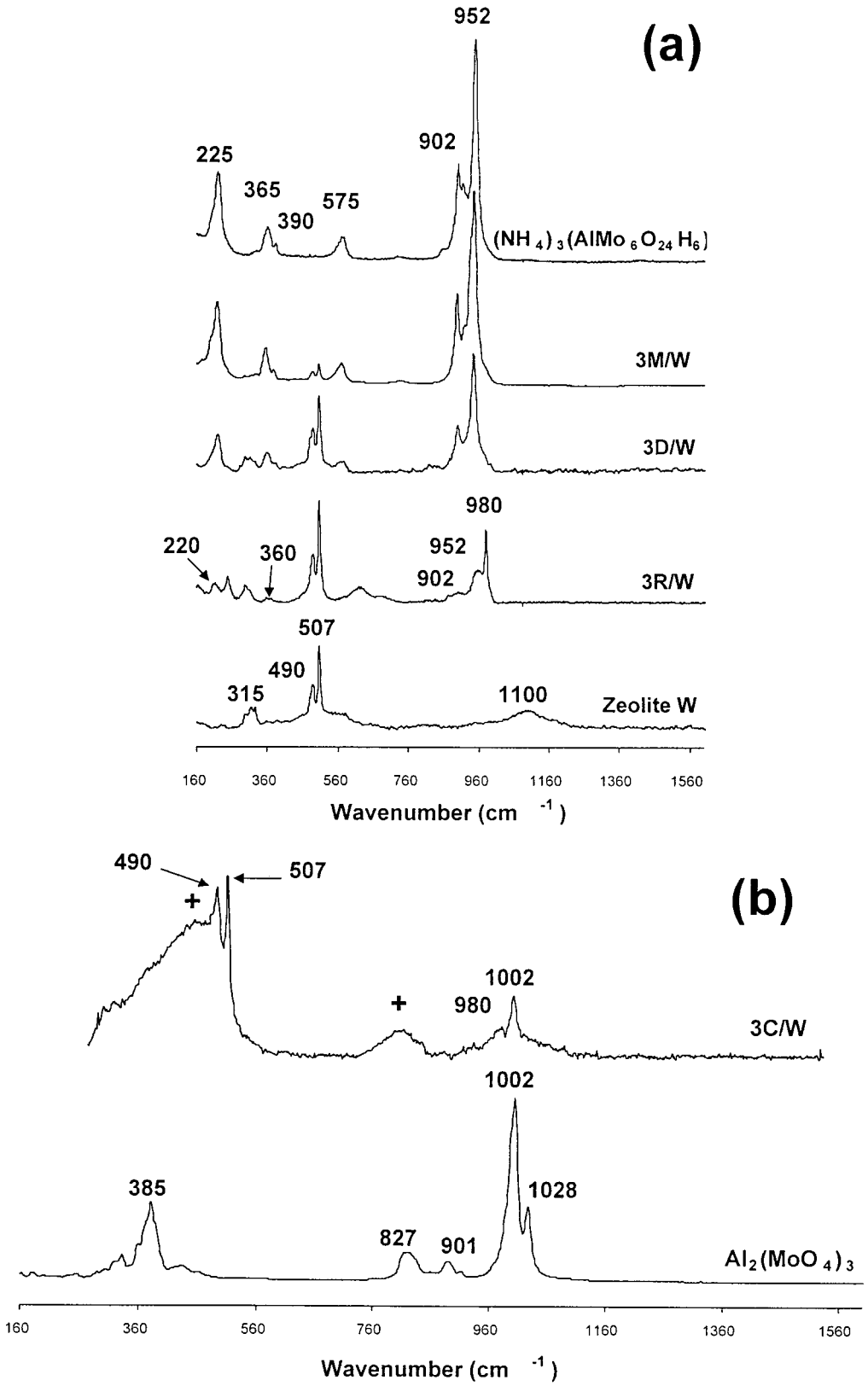

Figure 1. Raman spectra of (a) the nonloaded W zeolite, $AlMo_6$, 3M/W, 3D/W, and 3R/W, and (b) $Al_2(MoO_4)_3$ and 3C/W. +: lines of the glass of the Raman in situ cell.

the samples by solid state ^{95}Mo NMR. To address this question and to reinforce the Raman and NMR results, EXAFS and XANES studies have been carried out.

There are only a few studies in the literature that use the XANES at the Mo K- or L-edge to characterize the oxomolybdate supported phase. It has been shown that the distinction between octahedral and tetrahedral environments can be made through the shape of the Mo K-edge[27,28] or the splitting of the Mo L-edge.[29,30]

The Mo K- and L-edge XANES spectra of 3D/W and the Mo K-edge XANES spectrum of 3C/W are reported in Figure 4, in which are also reported the XANES spectra of reference

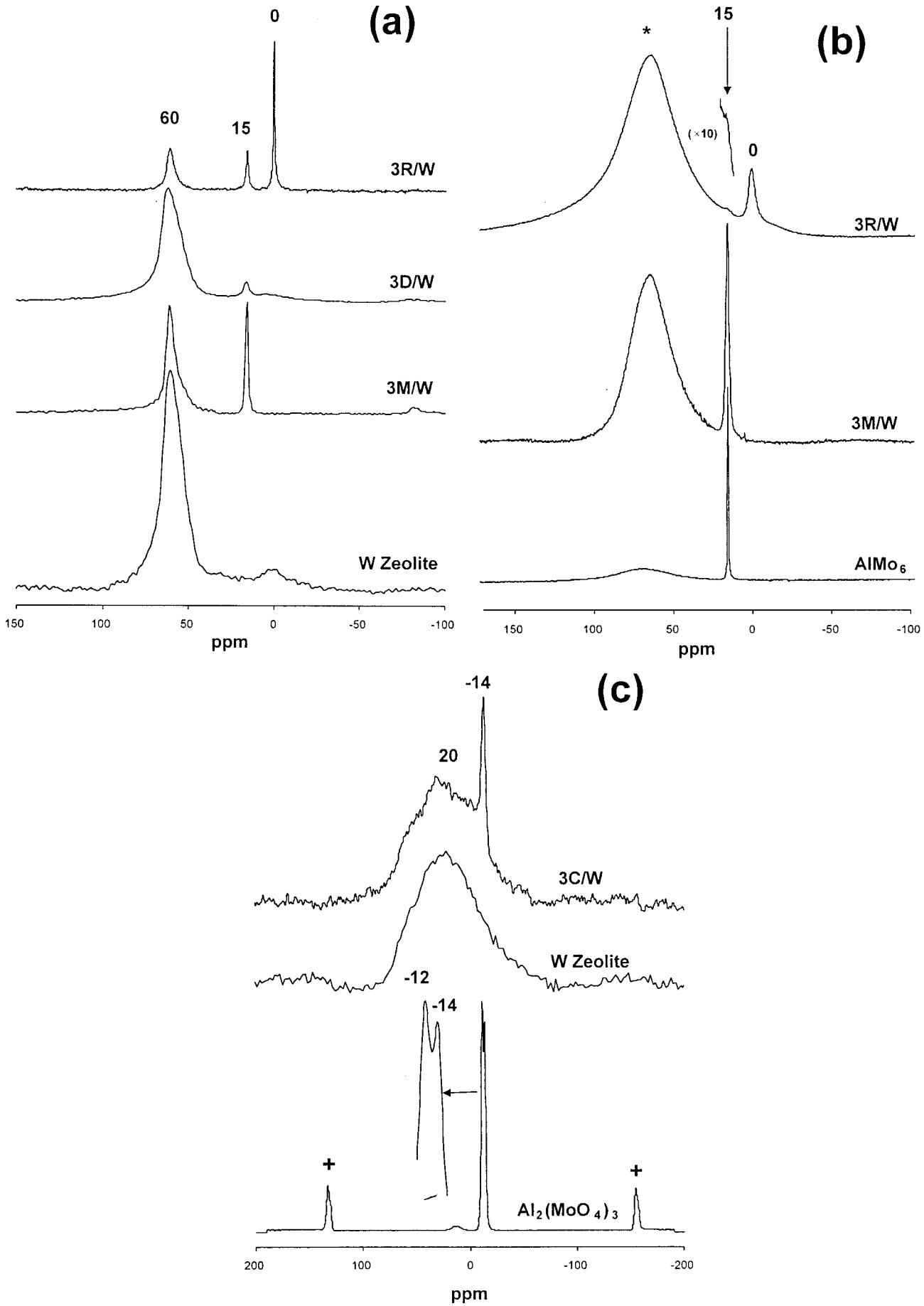

Figure 2. ^{27}Al NMR spectra of (a) the W zeolite, 3M/W, 3D/W, and 3R/W (MAS NMR), (b) $AlMo_6$, 3M/W, and 3R/W (liquid-state NMR), and (c) $Al_2(MoO_4)_3$, the dehydrated W zeolite and 3C/W (MAS NMR). * Probe signal of the spectrometer. +: rotation bands.

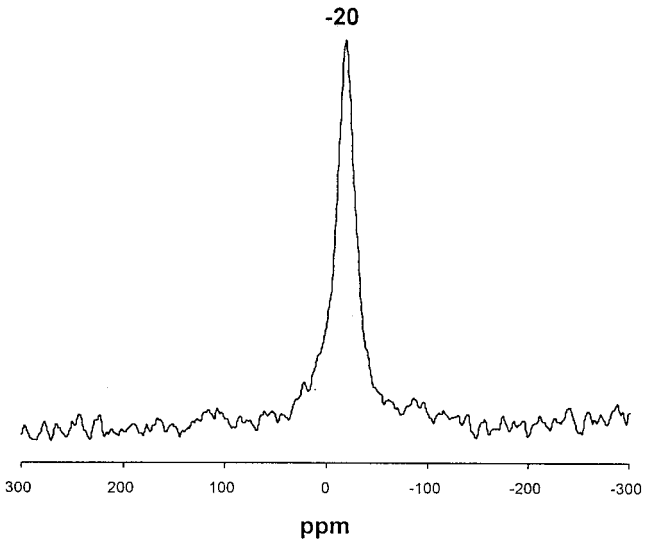

Figure 3. Liquid state ^{95}Mo NMR spectra of 3M/W.

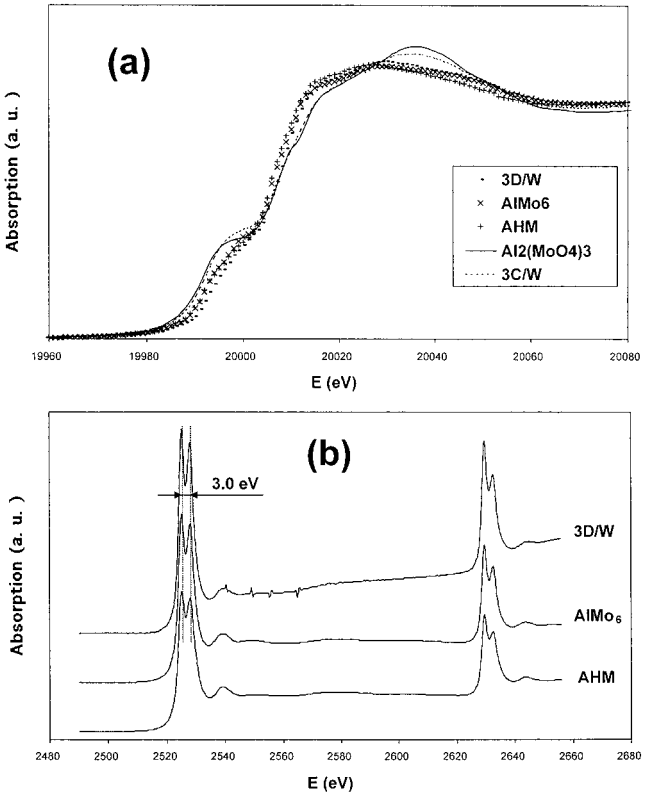

Figure 4. XANES spectra at the (a) Mo K-edge of 3D/W, 3C/W, $AlMo_6$, AHM, and $Al_2(MoO_4)_3$ and (b) Mo L-edge of 3D/W, $AlMo_6$, and AHM.

samples ($AlMo_6$, AHM, $Al_2(MoO_4)_3$). Unfortunately, the Mo K-edge spectra of $AlMo_6$ and of AHM (Figure 4a) are similar but look like that of 3D/W. We are here comparing two different distorted octahedral environments, and this difference is not easily seen with Mo K-edge signature. However, it can be noticed that the spectra of $Al_2(MoO_4)_3$ and 3C/W present a more pronounced preedge peak, which indicates a more distorted environment than in $AlMo_6$ or AHM. The Mo L-edge spectra of $AlMo_6$ and AHM (Figure 4b) are in agreement with previous studies on isopolymolybdates,[27,31] in which the authors showed that the splitting of the L_{II} and the L_{III} lines reflects the splitting of the d orbitals and thus the molybdenum environment symmetry. According to them, in octahedral environments, the most intense line of each edge should be the low energy one, and the splitting should range from 3.0 to 4.5 eV, which is the case here for 3D/W, $AlMo_6$, and AHM. The similarities of these spectra do not allow us to make the distinction between $AlMo_6$ and AHM and to use this technique to draw definitive conclusions on the nature of the supported oxomolybdate phase. Nevertheless, the Mo K-edge shows us very clearly that the species found after calcination is different from that identified on the dried sample, and that it seems similar to $Al_2(MoO_4)_3$.

EXAFS is thus needed to determine more clearly the structure of the supported oxomolybdate phase. The spectra of reference solutions ($AlMo_6$ and AHM), of a bulk reference $Al_2(MoO_4)_3$ and of the zeolite-supported samples are shown in Figure 5. The spectra of the references $AlMo_6$ and AHM have been recorded for the products in aqueous solution and bulk, with the aim of the work being to study the species in solution in the pores (for the matured and rehydrated states) and precipitated (for the dried and calcined states). Because they are similar, only the spectra of the references in aqueous solution are presented here. However, this shows that their structures are not affected by the dissolution of the ammonium salts.

The comparison between the EXAFS spectra and the corresponding Fourier transforms of the references and of the samples clearly shows that the signals obtained for the oxidic precursors in the matured, dried, and rehydrated states do not correspond to that of AHM. The RDF of AHM exhibits a second shell (Mo−Mo or Mo−Al) peak (2.4−3.8 Å, not phase corrected) that includes at least two different contributions. A study of the inverse Fourier transform of this region of the spectrum indicates that it must be the result of two types of molybdenum atoms corresponding to very close but different distances. This double contribution peak is not present on the spectra of the zeolite-supported samples, in any of the four states considered in this work: these show a peak (2.5−3.5 Å, not phase corrected) assignable to only one type of molybdenum neighbor. This simple comparison of the spectra clearly shows that the species present on the support at the various steps of the preparation of the oxidic precursor is never ammonium heptamolybdate. With the spectra presenting strong similarities with that of $AlMo_6$, it is now important to see whether 3M/W or 3D/W can be fitted with $AlMo_6$ contributions. Because of insufficient separation of the peaks corresponding to the oxygen neighbors (1.0−2.5 Å, not phase corrected) and the possible superposition in the second shell of both the Mo and the Al contributions, it was impossible to extract directly from the experimental spectrum of $AlMo_6$ the phase shift and backscattering amplitude functions needed for the fit.

The spectrum of the reference $AlMo_6$ compound has therefore been simulated with FEFF software,[18−21] with structural parameters issued from ADF (Amsterdam density functional program) calculations.[32] This will enable us to understand the details of the experimental spectrum presented in Figure 6. Here, we notice that the first peak, from 1.0 to 2.5 Å (not phase corrected), is due to three types of oxygen neighbors: 2 at 1.7340 Å, 2 at 1.9336 Å, and 2 at 2.3510 Å. This results in a very broad peak, in which the various contributions cannot be isolated, making it difficult to extract directly from the experimental spectrum the values that will help fit the spectra of the samples. This phenomenon is due to the fact that the oxygen is a light element, whose signals cannot be differentiated easily when the distances are so close. The second peak (2.5−3.5 Å, not phase corrected) includes both a Mo contribution (2 atoms at 3.3750 Å) and an Al contribution (1 atom at 3.3750 Å). For an easier understanding, these values are summarized in Table 2. Figure 6 shows the comparison between the

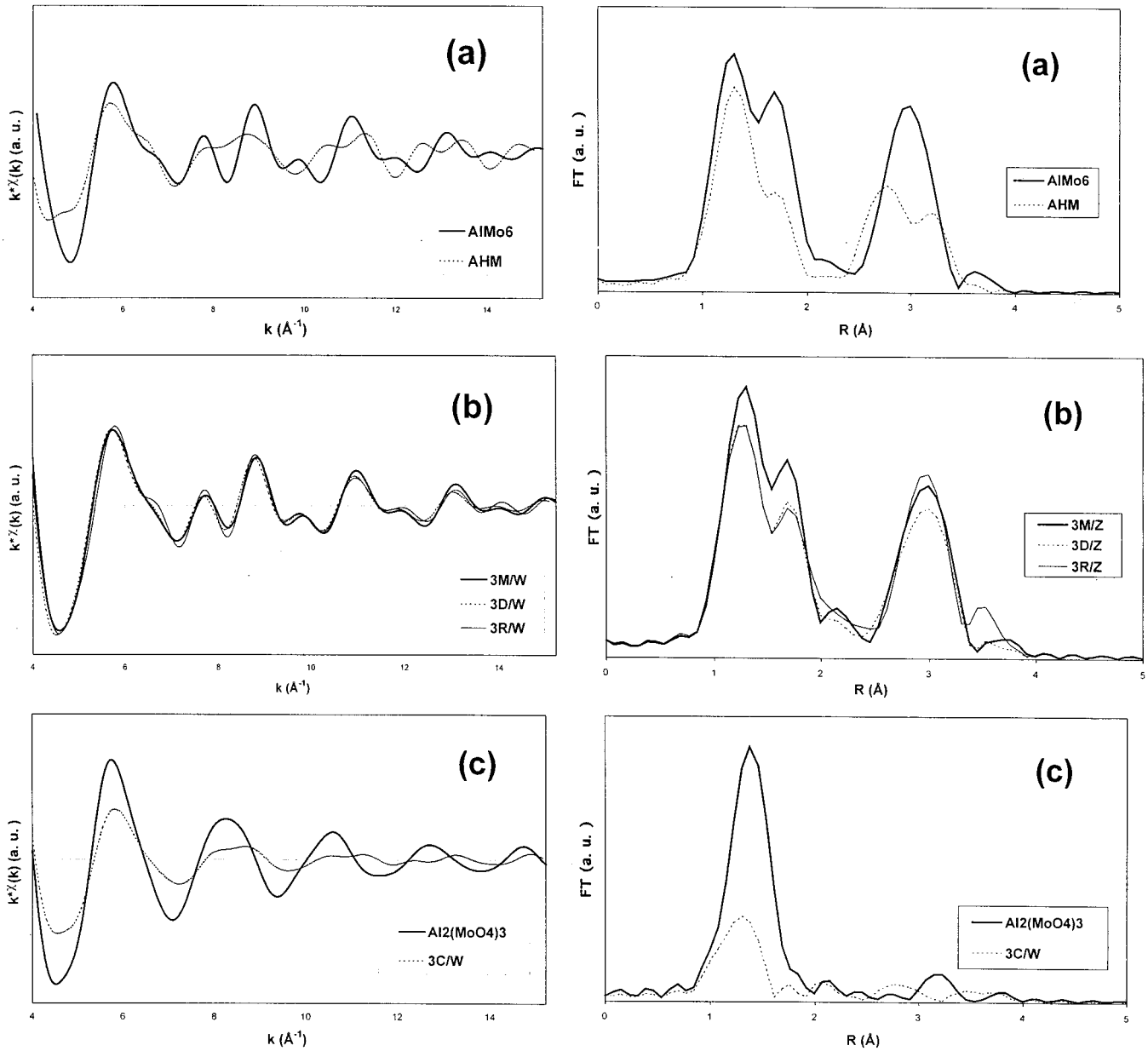

Figure 5. EXAFS spectra at the Mo K-edge (left) and Fourier transforms (right) of the three references and of the zeolite-supported samples: (a) $AlMo_6$ and AHM; (b) 3M/W, 3D/W, and 3R/W; and (c) $Al_2(MoO_4)_3$ and 3C/W.

experimental EXAFS signal of $AlMo_6$ and the simulation obtained using the FEFF-calculated contributions and the parameters reported in Table 3. The simulation is in good agreement with the experience, except for the Mo−Al distance which appears to be a little higher than expected by the calculation (3.46 vs 3.375).

These contributions were then used to fit the EXAFS spectra of the supported samples. The simulated spectra of 3M/W and 3D/W are very close to the experimental ones (see Figure 7), using parameters that match very well the structural data for $AlMo_6$ (see Table 4). These results confirm the presence of $AlMo_6$ on 3M/W and 3D/W. In addition, because the EXAFS signal is an averaged one, the detection of $AlMo_6$ on our samples proves that this species is majoritary.

The spectrum of the calcined sample 3C/W, recorded in situ (Figure 5c), is different from the spectra of $AlMo_6$ or AHM and closer to that of $Al_2(MoO_4)_3$. However, it appears that the latter is hardly usable as a reference: only one peak is detected in the Fourier transform (1.0−2.5 Å, not phase corrected), corresponding to the contributions of oxygen atoms. The contribution of the first Mo neighbors should appear after 4 Å, in a region where the noise is too strong to detect any signal. Consequently, only the contributions of the oxygen atoms can be used, whose analysis, as discussed above, is not precise when several close distances are present. It is thus not possible to use the EXAFS of $Al_2(MoO_4)_3$ to model the structure of the species, to fit the spectrum of our sample with its contributions. Given that the Mo K-edge XANES spectra of 3C/W and $Al_2(MoO_4)_3$ look very similar, the symmetries of the sample and of the reference must be also similar. Furthermore, the EXAFS spectrum (see fitting parameters in Table 5, obtained with McKale[34] calculated contributions) seems to indicate isolated tetrahedral molybdenum atoms, as in $Al_2(MoO_4)_3$. This is not enough to conclude, but it is an interesting clue to confirm the results of ^{27}Al NMR and Raman spectroscopies and indicate that the calcination of the Anderson entity leads to a species close to the aluminum molybdate.

The last step of this EXAFS study is the analysis of the rehydrated sample, 3R/W. As for the other samples, its spectrum is different from that of AHM. As expected, it is also different

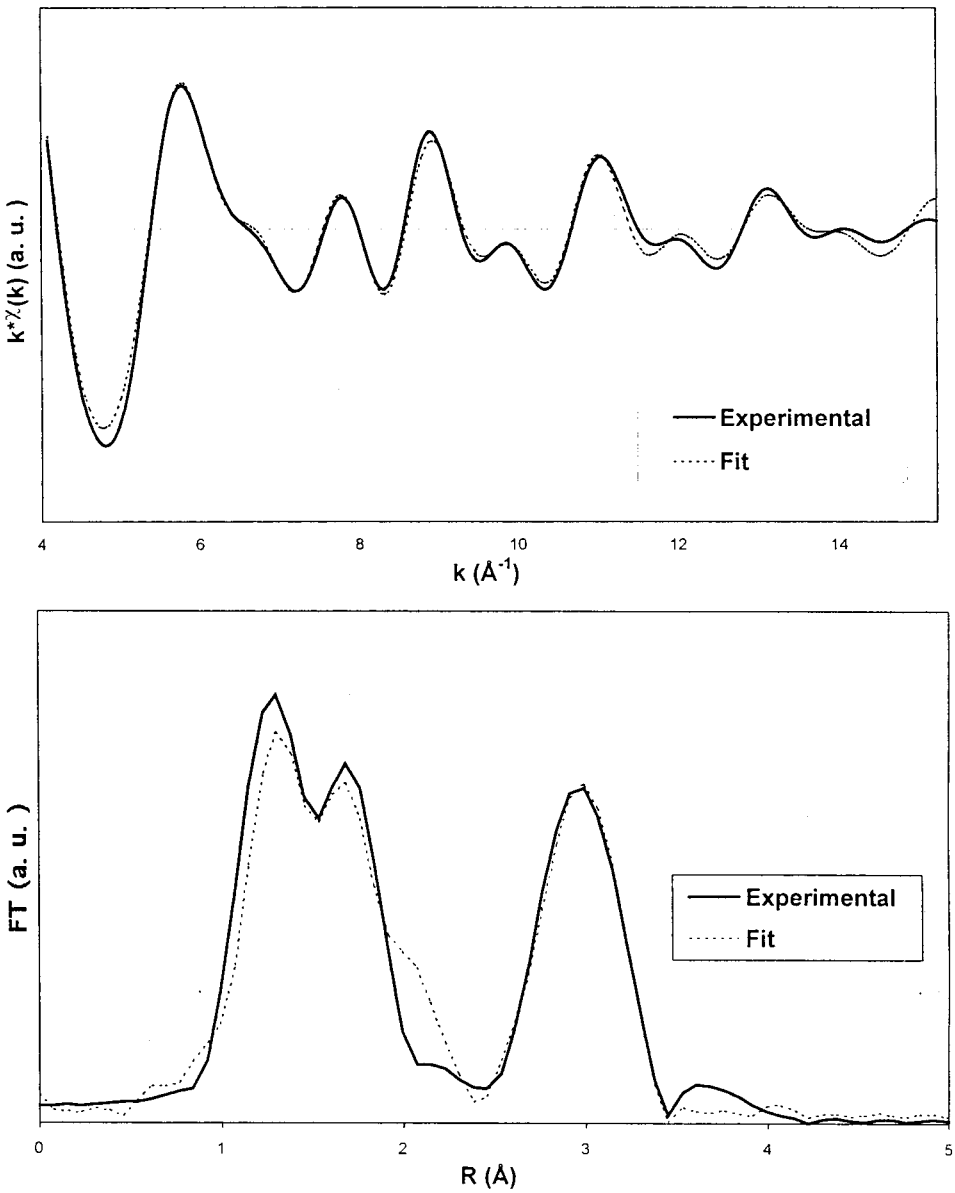

Figure 6. Comparison between the experimental EXAFS of $AlMo_6$ and its fit.

TABLE 2: Parameters of the FEFF Simulation of the $AlMo_6$ Reference

neighbor	O (1)	O (2)	O (3)	Mo	Al
number	2	2	2	2	1
distance (Å)	1.7340	1.9336	2.3510	3.3750	3.3750

TABLE 3: Fit Parameters for the Experimental $AlMo_6$ EXAFS Signal with the Contributions Calculated by FEFF[a]

	Mo−O (1)	Mo−O (2)	Mo−O (3)	Mo−Mo	Mo−Al
N	2.0	2.0	2.0	2.2	1.0
$\Delta\sigma$ (Å)	0.02	0.06	0.06	0.06	0.02
R (Å)	1.72	1.92	2.34	3.33	3.46
ΔE (eV)	5.4	5.4	5.4	5.4	5.4

[a] N: ±10%. $\Delta\sigma$: ±0.01 Å. R: ±0.02 Å. ΔE: ±0.1 eV.

from that of $Al_2(MoO_4)_3$: it is generally accepted in the literature[36] that this surface species disappears as soon as the sample is put back to ambient air. The spectrum of 3R/W is very similar to those of 3M/W, 3D/W, and $AlMo_6$. Yet, there are some differences that make it impossible to fit with the contributions of $AlMo_6$. These differences are visible as a new peak in the Fourier transform (3.3−3.8 Å, not phase corrected, see Figure 5b) and may arise from the presence of another entity. This is in agreement with the NMR results which had shown that the rehydration process led to a reformation of the Anderson entity from surface "$Al_2(MoO_4)_3$", and also with the Raman results that revealed a line not due to $AlMo_6$. As neither liquid nor solid-state ^{27}Al NMR detected any other species on this sample, the polymolybdate phase detected by Raman spectroscopy must contain no aluminum.

To sum up, ^{27}Al NMR has confirmed and completed the Raman results: the impregnation of a stabilized HY zeolite with an ammonium heptamolybdate solution leads to a reaction in solution with the Al^{3+} ions, to form an Anderson heteropolyanionic entity $AlMo_6O_{24}H_6^{3-}$ by extracting aluminum atoms from the support. This entity is precipitated on the support during the drying treatment, and upon calcination, a dispersed aluminum molybdate phase appears. The rehydration allows a partial reformation of the Anderson entity in solution and in a precipitated form. EXAFS has enabled further confirmation of these results and shown that the aluminomolybdate anion is the major phase present on the zeolite in the matured and dried states. It has also shown that the rehydration is a complex process at the end of which the nature of the supported entities is not clearly defined.

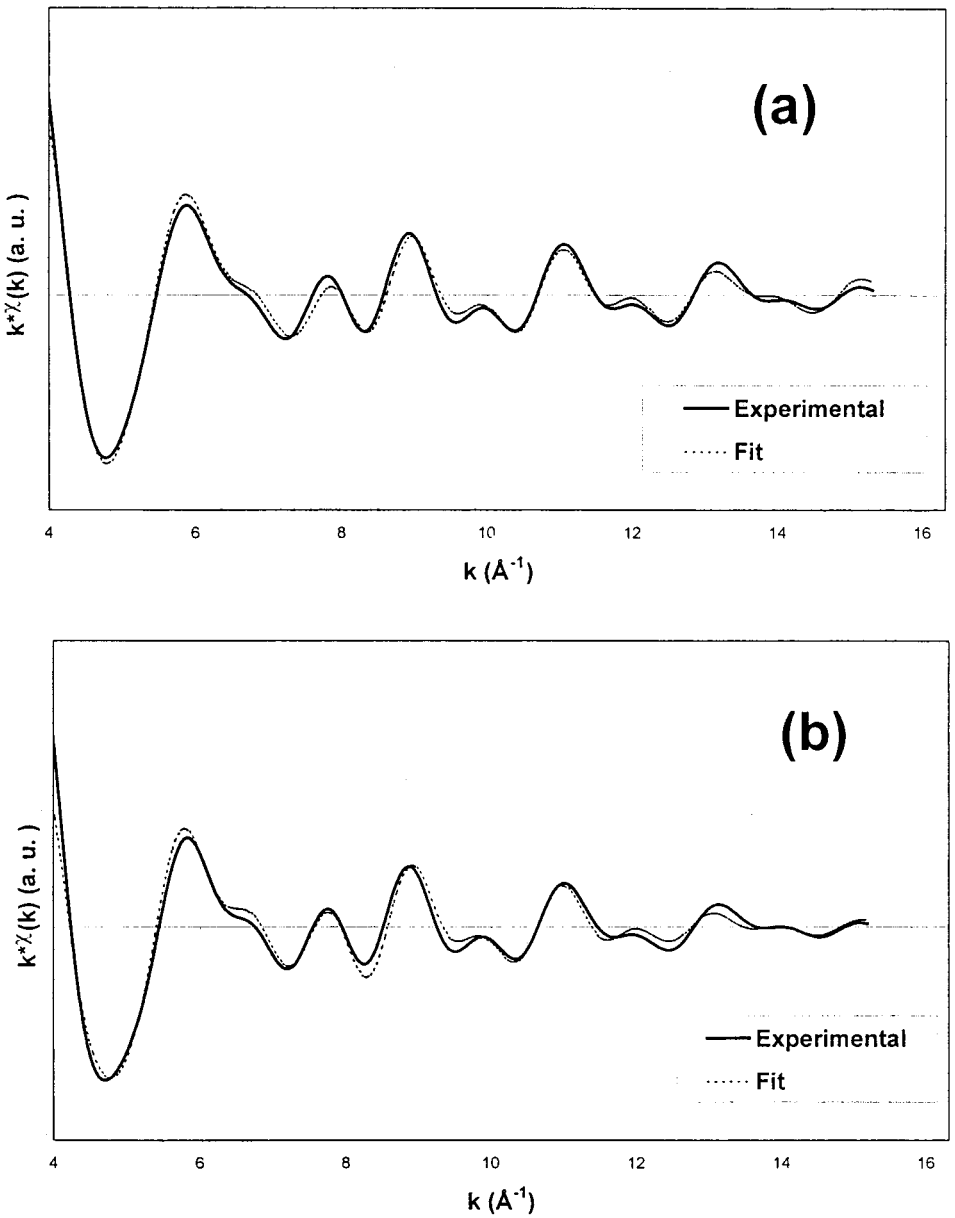

Figure 7. Comparison between the experimental spectra of (a) 3M/W and (b) 3D/W and their fits.

TABLE 4: Fitting Parameters of 3M/W and 3D/W[a]

		Mo−O (1)	Mo−O (2)	Mo−O (3)	Mo−Mo	Mo−Al
3M/W	*N*	2.0	2.0	2.0	1.7	1.1
	Δσ (Å)	0.04	0.06	0.08	0.07	0.10
	R (Å)	1.73	1.95	2.37	3.36	3.54
	Δ*E* (eV)	7.3	7.3	7.3	7.3	7.3
3D/W	*N*	2.0	2.0	2.0	2.2	1.0
	Δσ (Å)	0.06	0.08	0.07	0.08	0.08
	R (Å)	1.72	1.97	2.35	3.36	3.50
	Δ*E* (eV)	3.7	3.7	3.7	3.7	3.7

[a] *N*: ±10%. Δσ: ±0.01 Å. *R*: ±0.02 Å. Δ*E*: ±0.1 eV.

TABLE 5: Fitting Parameters of 3C/W[a]

	N	Δσ (Å)	*R* (Å)	Δ*E* (eV)
Mo−O	3.8	0.07	1.77	5.0

[a] *N*: ±10%. Δσ: ±0.01 Å. *R*: ±0.02 Å. Δ*E*: ±0.1 eV.

Origin of the Aluminum Atoms. We have seen that formation of the Anderson entity takes place during the impregnation, but it is not clear yet where the aluminum atoms necessary to this reaction come from. A plausible suggestion can be made from the parallel between the phenomenon observed in the impregnation of an alumina and the presence of amorphous alumina in the zeolite, but it is not obvious that the aluminum atoms come from there and not from the zeolite structure.

The first observation that can be made to stress the role of the octahedral Al atoms in the formation of the Anderson heteropolyanion is the disappearance of the corresponding MAS NMR line at 0 ppm on the spectra of the matured and dried samples 3M/W and 3D/W (see Figure 2b). Furthermore, the line around 1100 cm^{-1} in Raman spectroscopy observed for the zeolite (Figure 1), assigned to the presence of amorphous alumina[22] (as will be confirmed later), disappears for the impregnated sample. The Al^{3+} ions used to form the Anderson aluminomolybdate anion may originate from these entities, the localization of which has been recently studied by Gola et al.[35] and Menezes et al.[36]

We now consider two other loadings of molybdenum (5 and 8 wt %) to see the evolution of the previous observations. Because we have seen that the species observed in the matured state are conserved in the dried state, we will not present all of the spectra for both states. Figure 8 presents the Raman spectra

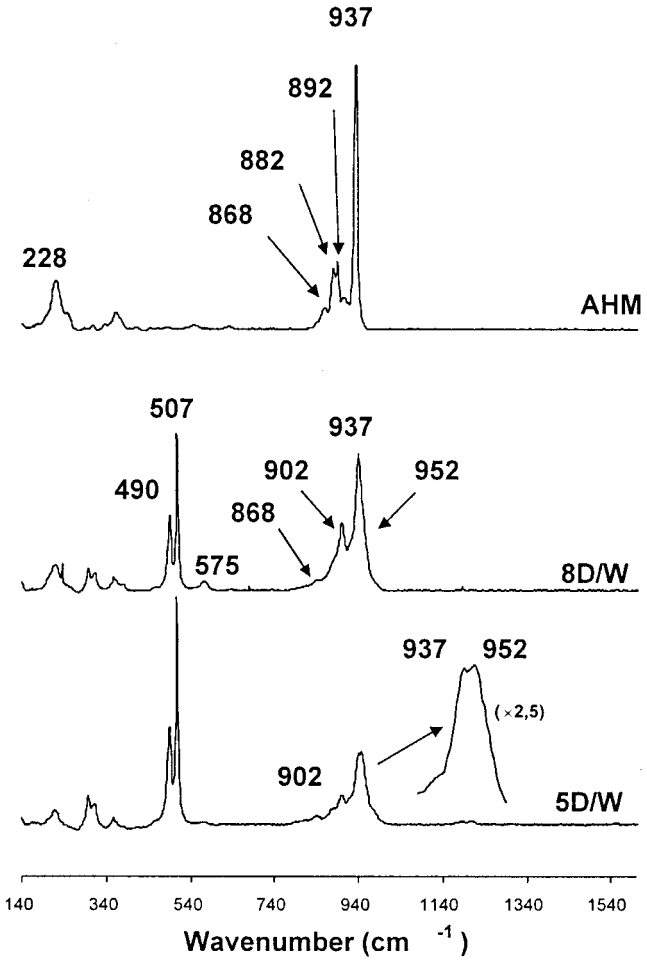

Figure 8. Raman spectra of 5D/W, 8D/W, and AHM.

of 5D/W and 8D/W together with that of AHM. The Raman spectrum of AHM exhibits a main line at 937 cm^{-1} and secondary ones at 892, 882, 868, 555, and 635 cm^{-1}. The line at 228 cm^{-1} cannot be considered as characteristic, because it is also present for $AlMo_6$, the Raman features of which are described above. The Raman spectrum of 5D/W exhibits the lines of the zeolite at 507, 490, 315, and 295 cm^{-1}, together with a broad line with two contributions at 952 and 937 cm^{-1}, i.e., the characteristic main lines of respectively $AlMo_6$ and AHM. A secondary line of $AlMo_6$ can be seen as a small peak at 902 cm^{-1}, and also a secondary line of AHM is present as a shoulder at 868 cm^{-1}. The lines of the zeolite are also observed for 8D/W, but here the main line is located at 937 cm^{-1}, with a shoulder on the high wavenumber side, which can be assigned to the simultaneous presence of AHM and $AlMo_6$, respectively. The presence of the Anderson entity in both samples is confirmed by the line at 575 cm^{-1} and also by ^{27}Al MAS NMR spectroscopy (see Figure 9), the spectra of which exhibit the characteristic line at 15 ppm. The coexistence of $AlMo_6$ and AHM is also partly confirmed by liquid-state ^{95}Mo NMR of 5M/W and 8M/W (see Figure 10). The spectrum of 5M/W exhibits three lines, at 33 ppm (assigned to AHM, according to the literature[7]), 0 ppm (assigned to MoO_4^{2-}), and −20 ppm (assigned to $AlMo_6$). The presence of MoO_4^{2-} ions is due to a dissociation equilibrium of AHM and $AlMo_6$. The spectrum of 8M/W exhibits only two distinct peaks, at 33 and 0 ppm, characteristic of AHM and MoO_4^{2-}, respectively, with a shoulder around −20 ppm which indicates here the presence of $AlMo_6$, but clearly, AHM is preponderant for higher Mo loadings.

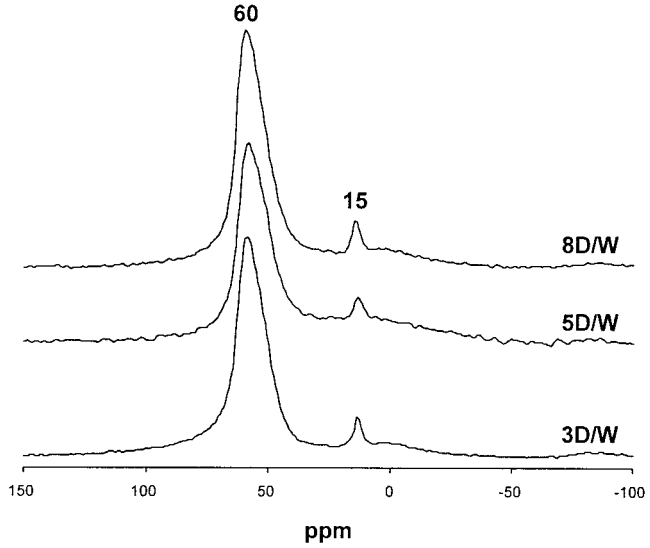

Figure 9. ^{27}Al MAS NMR spectra of 3D/W, 5D/W, and 8D/W.

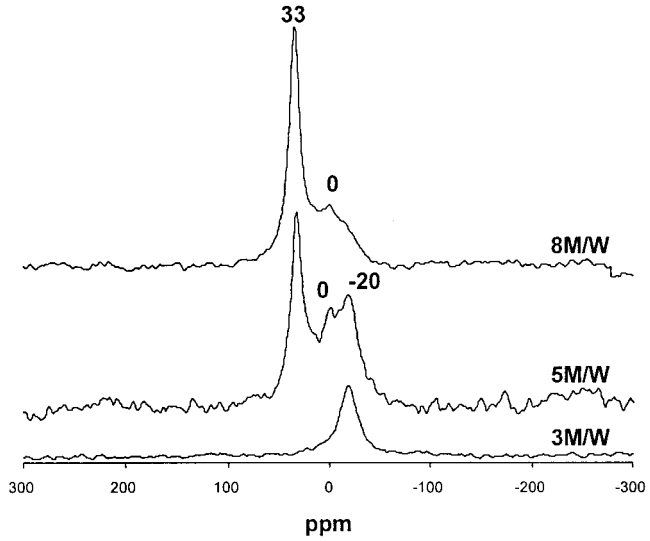

Figure 10. Liquid state ^{95}Mo NMR spectra of 5M/W and 8M/W.

These results indicate that the first phenomenon to occur upon impregnation is the formation of the Anderson entity, but concurrently, precipitation of AHM takes place for high Mo loadings. Upon calcination, AHM will lead to well crystallized molybdenum oxide MoO_3 (main lines in Raman at 995 and 818 cm^{-1}, spectrum not reported here[37]). The Raman spectra show that AHM becomes increasingly preponderant as the loading increases. It seems therefore that a limited quantity of $AlMo_6$ can be formed, that precipitation of AHM occurs when this limit is reached (at 3 wt %), and that, thereafter, the higher the loading, the more AHM precipitates. This tends to indicate that there is also a limited quantity of aluminum atoms available to form the aluminomolybdate anion. We now need to establish whether this limit is the quantity of nonframework aluminum atoms.

We therefore used the S zeolite, that was not acid washed, and which consequently offers more extraframework aluminum atoms: for the same structural (Si/Al) ratio as the W zeolite (19, see Table 1), it has a lower bulk (Si/Al) ratio (2.8 compared with 13.6 for the W zeolite). This is confirmed by its ^{27}Al NMR spectrum (Figure 11), where the peak at 5 ppm, characteristic of the nonframework aluminum atoms, is more intense than in the case of the W zeolite (Figure 2b). Figure 11 also presents the spectra of samples 3D/S, 5D/S, 8D/S, and 15D/S. They all

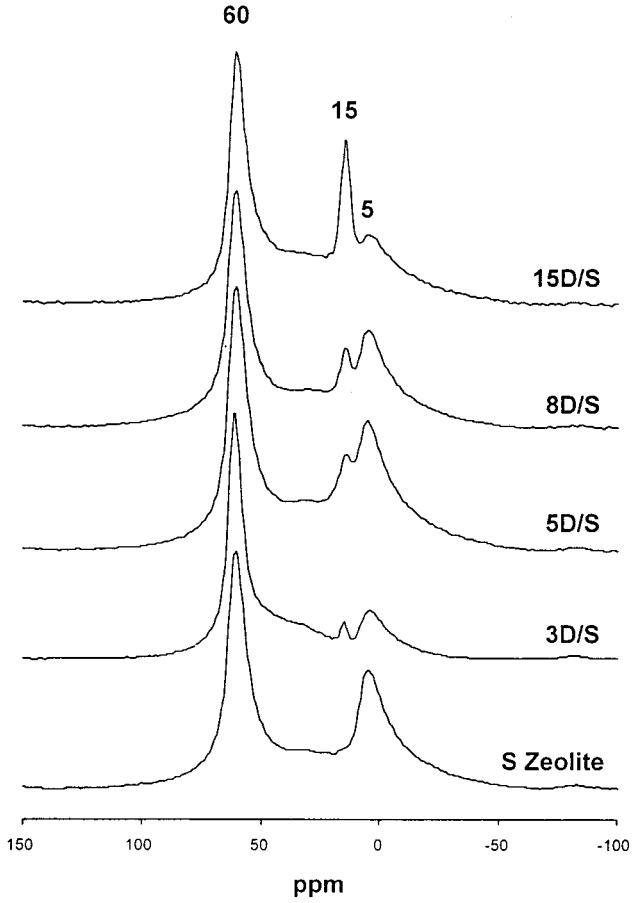

Figure 11. ^{27}Al MAS NMR spectra of the S zeolite, 3D/S, 5D/S, 8D/S, and 15D/S.

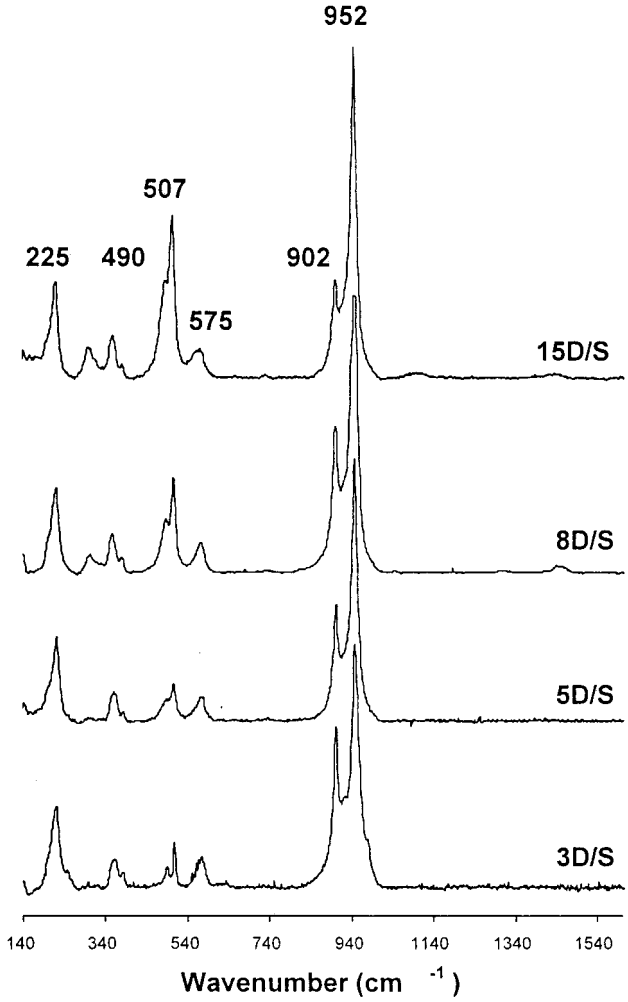

Figure 12. Raman spectra of 3D/S, 5D/S, 8D/S, and 15D/S.

exhibit the two peaks characteristic of the zeolite together with the one characteristic of $AlMo_6$ at 15 ppm. This confirms the formation of $AlMo_6$, but we need Raman to know whether AHM has precipitated or not. These Raman spectra are shown in Figure 12. Contrarily to the previous results of 5D/W and 8D/W, none of these spectra exhibit the characteristic lines of AHM, but they all show very clearly the different peaks assigned to crystalline $AlMo_6$. When the number of extraframework aluminum atoms is increased, the precipitation of AHM is delayed. Consequently, we can assert that the nonframework aluminum atoms are necessary to form the Anderson entity and that if they are present in sufficient quantities the formation of the aluminomolybdate anion occurs preferentially to the precipitation of AHM.

The last step to confirm this assumption is to use a zeolite that offers no extraframework aluminum atom and to see whether $AlMo_6$ is formed or not. This was done using a steamed, EDTA-treated, and NH_4NO_3-exchanged zeolite (E), which has been prepared according to the work of Gola et al.[35] The E zeolite, according to the comparison of its bulk and structural (Si/Al) ratios (see Table 1), should present no nonframework aluminum atom. However, these ratios are determined at ± 0.6, and the washing treatments are often incomplete and may leave a small amount of amorphous alumina on the zeolite. This is the case here, as shown by the ^{27}Al NMR spectrum of the E zeolite presented in Figure 13. Together with the peak at 60 ppm assigned to the tetrahedral aluminum atoms of the structure of the zeolite, a very weak peak at 0 ppm can be seen. Figure 13 also presents the spectrum of 3D/E. As expected, the peak at 0 ppm totally disappears and is replaced by another at 15 ppm, characteristic of $AlMo_6$, which is also very weak, and

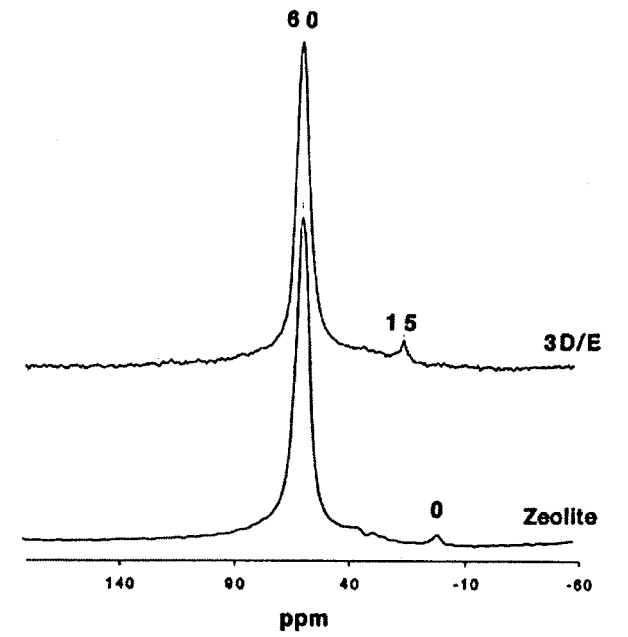

Figure 13. ^{27}Al MAS NMR spectra of the E zeolite and 3D/E.

whose intensity has to be compared with those of the peaks previously observed (Figures 2b, 9, and 11). The Raman spectra (Figure 14) give further evidence. First, the spectrum of the E zeolite confirms the assignment of the broad line observed at 1100 cm^{-1} for the W zeolite to an amorphous alumina phase:

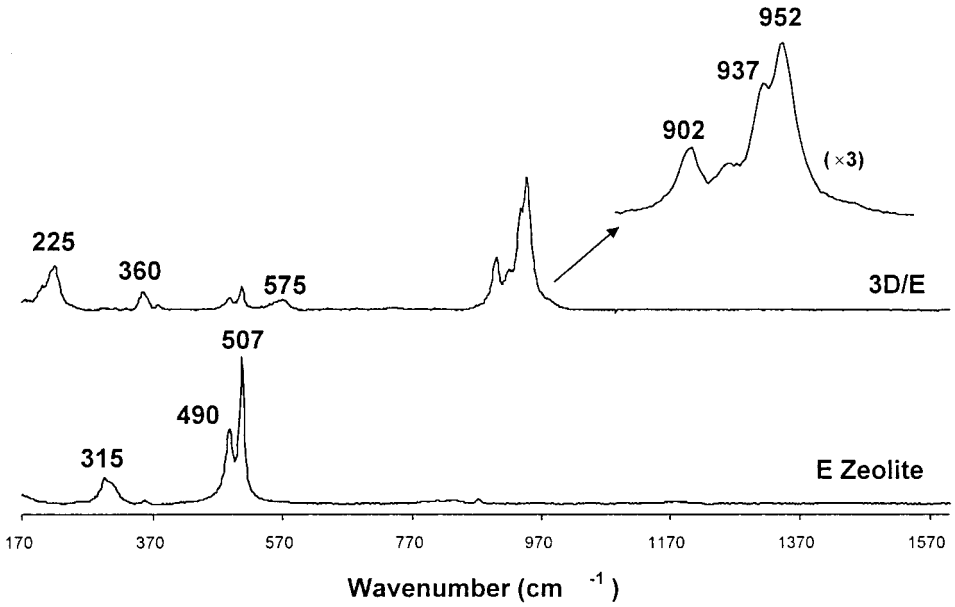

Figure 14. Raman spectra of the E zeolite and 3D/E.

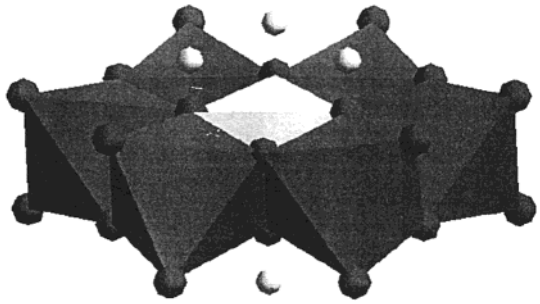

Figure 15. Representation of the structure of the Anderson entity. Six edge sharing MoO_6 octahedra surround an AlO_6 polyhedra on which are located six nonacid protons.

now that there are very few nonframework aluminum atoms, the line is absent. The spectrum of 3D/E presents the same kind of line as was observed for 5D/W (Figure 8): a broad line, apparently composed of two poorly resolved components, at 952 and 937 cm^{-1}, indicating respectively the formation of $AlMo_6$ and the precipitation of AHM. Precipitation of AHM was previously not observed below 5 Mo wt %. For the E zeolite, there are fewer nonframework aluminum atoms in an amorphous phase, and precipitation of AHM occurs earlier. Consequently, we can say that the very low amount of $AlMo_6$ formed is due to the very small quantity of aluminum atoms that remained on the zeolite in an amorphous phase. Apart from that, no atom from the structure seems to have been extracted to give the $AlMo_6$ structure.

These comparisons between different Mo loadings and supports allow us to conclude that the formation of the Anderson entity upon the impregnation of a zeolite with an AHM solution occurs through the extraction of the nonframework aluminum atoms present in the zeolite.

Localization of the Anderson Entity. Now that we know what is formed upon impregnation and how it is formed, we should consider where the Anderson entity is located on or inside the zeolite. Figure 15 shows a representation of this entity, which is a flat structure consisting of six molybdenum octahedra surrounding an aluminum atom. This entity formed upon impregnation can be located in the extragranular porosity as well as in the intragranular porosity, composed of three kinds of cavities[38]: the sodalite cavities, the prismatic cavities, and the supercages. However, the diameter of the $AlMo_6$ anion (around 7 Å) is larger than the size of the sodalite and prismatic cavities (6.6 and 2.2 Å, respectively), as is the size of the heptamolybdate anion. Consequently, only the supercages or the extragranular porosity contain enough space for an Anderson entity. As aforementioned, the aluminomolybdate anion is formed by extraction of nonframework aluminum atoms which can be located outside or inside the zeolite porosity,[35,36] through dissolution of Al^{3+} into the solution present in the pore according to the following equation:

$$6Mo_7O_{24}^{6-} + 24H_2O + 7Al^{3+} \leftrightarrow 7AlMo_6O_{24}H_6^{3-} + 6H^+$$

To distinguish between these two possibilities (localization in the extra granular porosity or inside the supercages), we have considered another type of preparation: MoO_3 vapocondensation. Recently, Iglesia et al.,[41−43] as well as other authors,[42] claimed that molybdenum can be located inside the supercage by vapocondensation of MoO_3. This sample 2V/W has been characterized by XRD, by ^{27}Al NMR, and by XANES and EXAFS at the Mo K-edge. The loading of 2% has been chosen in order to avoid any precipitation of MoO_3 on the zeolite.

The XRD experiments were carried out on samples 2V/W and 3D/W. The XRD patterns of these two samples are different. The comparison between these samples and the zeolite is presented in Figure 16. For 2V/W, only the lines of the support are observed but with a small shift and with variation in their relative intensities. The deduced unit cell parameter of the zeolite in 2V/W is 24.41 ± 0.02 Å, compared with 24.30 ± 0.02 Å for the nonloaded zeolite. These modifications indicate the presence of Mo species in crystallographic sites inside the supercages of the support. This clearly shows the location of the species inside the intragranular porosity of the zeolite. On the contrary, for 3D/W, the position and the relative intensities of the lines of the support are the same as those of the nonloaded zeolite, even if the overall intensities are lower due to absorption of signal by molybdenum. In addition, peaks characteristic of the aluminum Anderson salt of ammonium are observed in 3D/W (2θ at 8.32, 11.58, 15.00, 16.68, 25.14, and 29.22°). The

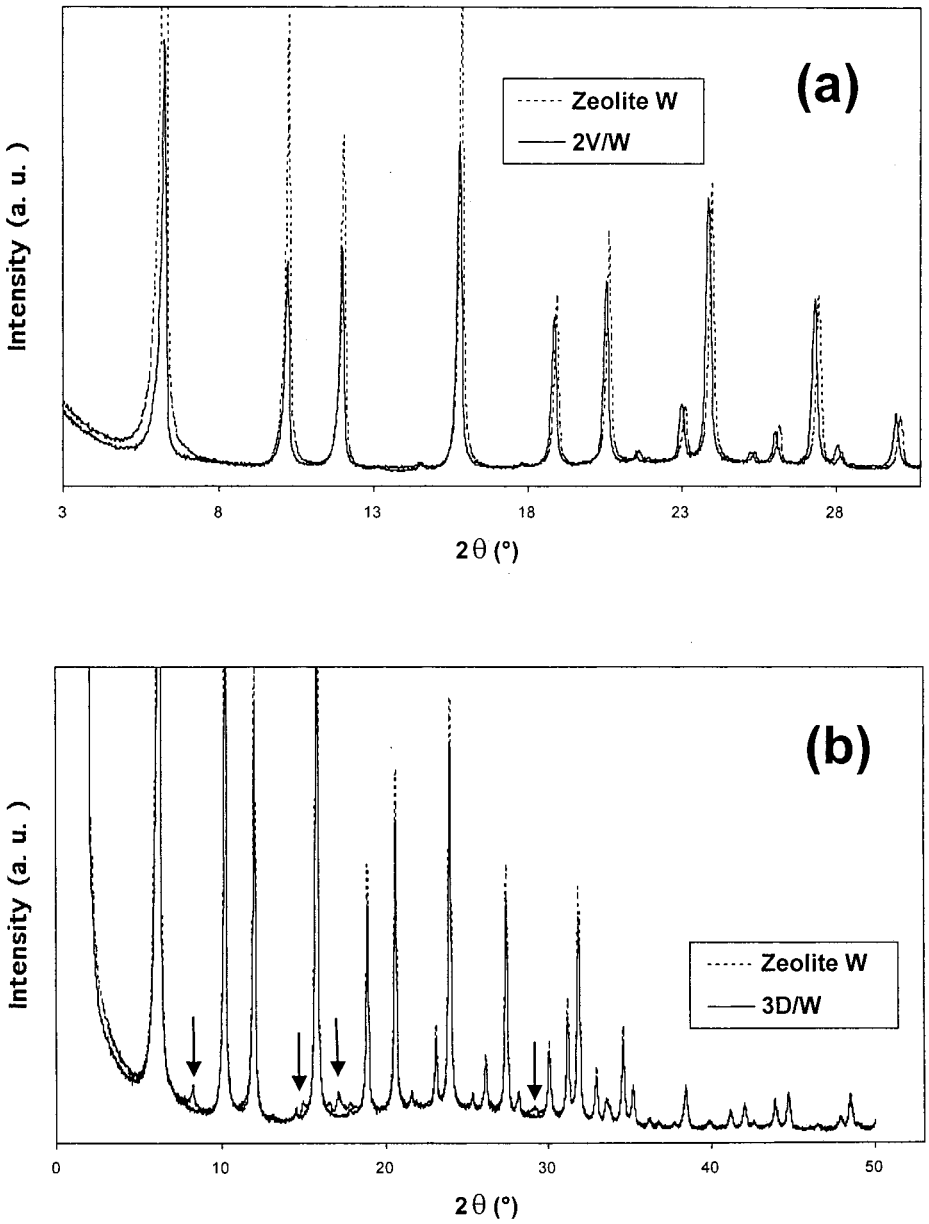

Figure 16. Comparison between the XRD spectra of the W zeolite with (a) 2V/W and (b) 3D/W. The arrows indicate the most visible lines of $AlMo_6$.

sharpness of these lines indicates at least 500 Å sized particles, which are too large to be located in the supercages. There could also be some $AlMo_6$ inside the supercages, but as no variation of the cell parameter and relative intensities is observed, we can conclude that the Mo species that are formed are mainly deposited outside the supercages of the zeolite.

This is in agreement with NMR and EXAFS results. The in situ ^{27}Al MAS NMR spectrum of 2V/W (Figure 17) exhibits only the broad peak around 20 ppm, corresponding to the dehydrated zeolite. The features of $Al_2(MoO_4)_3$, a species formed upon calcination of the impregnated samples as aforementioned, are not observed. The Mo K-edge XANES spectra of $AlMo_6$, MoO_3, and 2V/W (Figure 18) are similar but not identical, in particular the absorption edge of 2V/W appears at lower energy. Nevertheless, these spectra bring further confirmation of the NMR results: the shapes of the preedge peaks are different for 2V/W and $Al_2(MoO_4)_3$, showing the absence of the latter in the sample. The EXAFS spectrum of 2V/W (Figure 19) is clearly different from that of $Al_2(MoO_4)_3$ and MoO_3. The spectrum of 2V/W presents some similarities with that of $AlMo_6$.

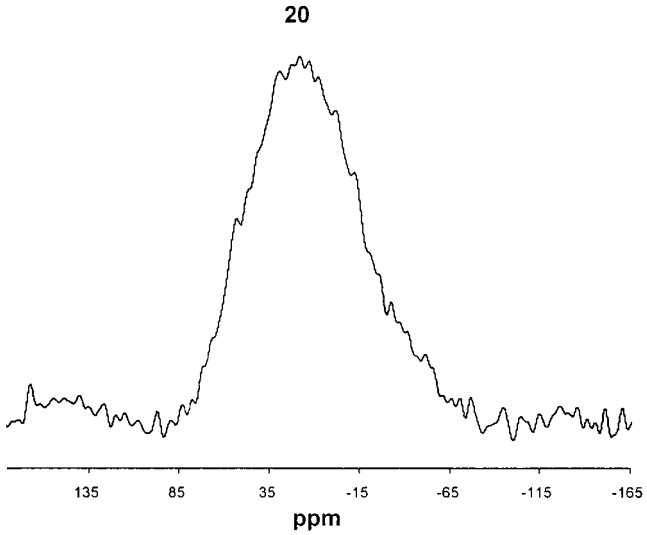

Figure 17. ^{27}Al MAS NMR spectrum of 2V/W.

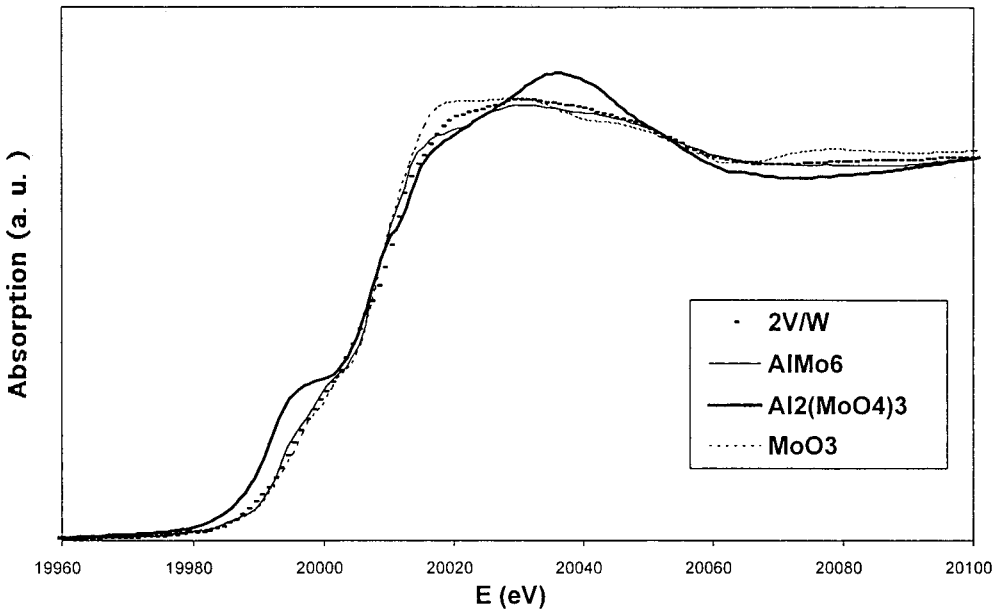

Figure 18. Mo K-edge XANES spectra of 2V/W, $AlMo_6$, MoO_3, and $Al_2(MoO_4)_3$.

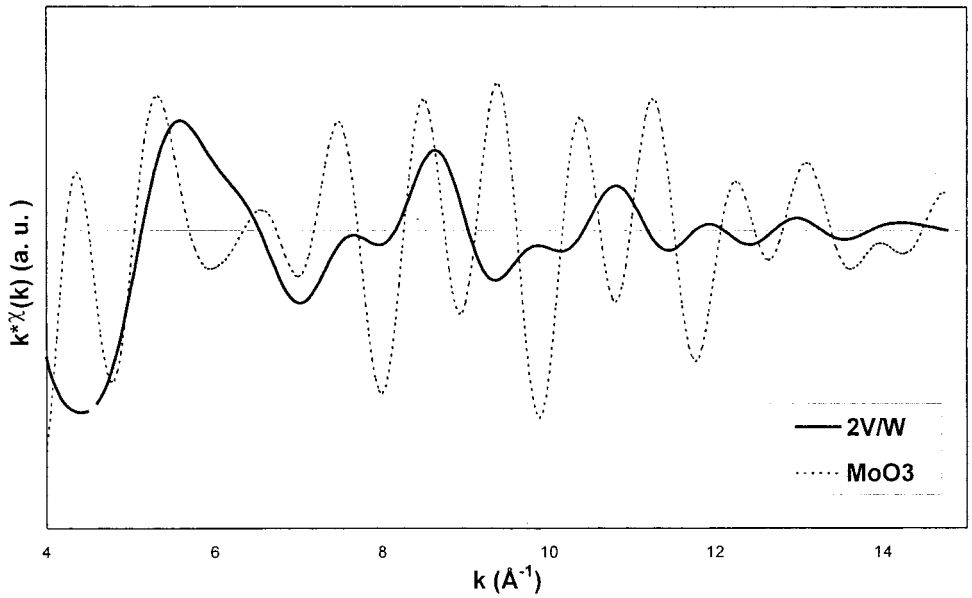

Figure 19. Mo K-edge EXAFS spectra of 2V/W and MoO_3.

However, the strong difference of the shapes of the first oscillation is significant, and the fit of the spectrum confirms that the supported species differs from $AlMo_6$. The comparison between the experimental spectrum and its fit realized with simple calculated contributions is shown in Figure 20. Four contributions are necessary to fit this spectrum: two types of oxygen atoms, one type of silicium or aluminum atom, and one type of molybdenum atom. The fitting parameters are presented in Table 6. These results indicate that the species supported on the zeolite consist of dimers (approximately one molybdenum neighbor), which are in vicinity of the framework. This is shown by the Mo−Si(Al) contribution and confirmed by the total number of oxygen neighbors, which is high for a dimeric species and which must include some contributions of oxygen atoms from the framework. Unfortunately, because of fluorescence, it has not been possible to characterize this solid by Raman spectroscopy. However, it appears that at high temperature, MoO_3 is vaporized and some Mo entities are transferred inside the supercages. Such a transfer can be due to the formation of molybdic acid and/or oxocation at high temperatures.[43] Thus, it can also be deduced that MoO_3 formed at high Mo loadings after consumption of the extraframework Al atoms (in the incipient wetness impregnation) might penetrate inside the supercages upon a high-temperature treatment.

Briefly, this preparation has enabled us to characterize the EXAFS signal of species located in the supercages. This signal is different from that found for the impregnated sample. These species are dimers, which is not the case of the Anderson entity, and their location inside the supercages, very close to the structure of the zeolite, induces a Mo−Si(Al) contribution in the EXAFS signal that has not been seen in the EXAFS signal of the impregnated samples. Consequently, this argues in favor of a conclusion that the aluminomolybdate anions identified above by several techniques are located in the extragranular porosity of the support.

The XRD, NMR, and EXAFS results allow us to conclude that the Anderson entities formed upon impregnation are not located inside the supercages. This is coherent with the fact

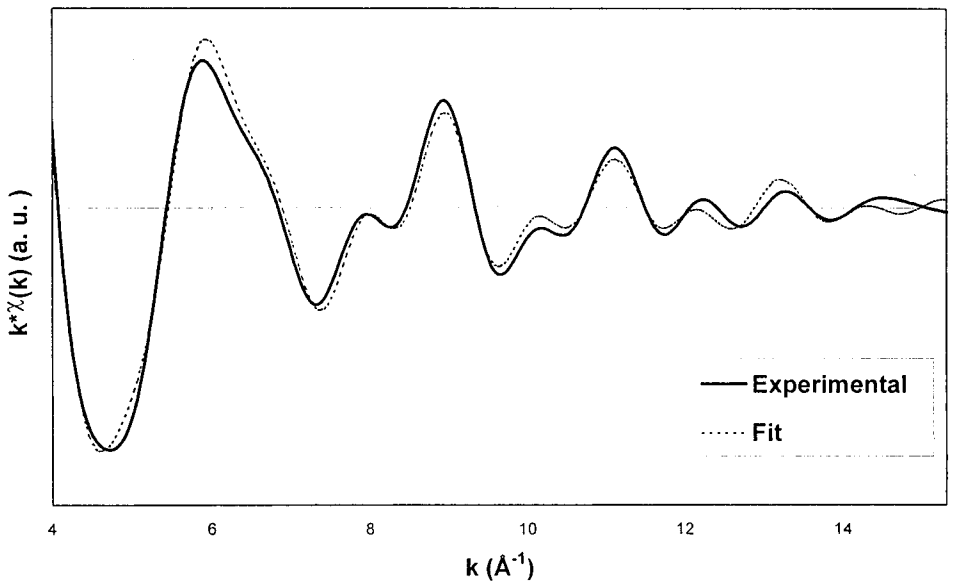

Figure 20. Comparison between the experimental EXAFS of 2V/W and its fit.

TABLE 6: Fitting Parameters of 2V/W[a]

	Mo−O (1)	Mo−O (2)	Mo−Si	Mo−Mo
N	3.7	1.8	0.7	1.3
$\Delta\sigma$ (Å)	0.08	0.08	0.05	0.07
R (Å)	1.72	1.96	2.60	3.31
ΔE (eV)	1.0	1.0	1.0	1.0

[a] *N*: ±10%. $\Delta\sigma$: ±0.01 Å. *R*: ±0.02 Å. ΔE: ±0.1 eV.

that the inside of the supercages is strongly acidic and negatively charged, whereas $AlMo_6$ is only stable in a pH range from 2 to 6[44] and is also negatively charged. It also can be noticed that the sharpness of the peak observed in NMR tends to indicate that the observed species does not undergo any confinement. Finally, we have detected $AlMo_6$ in liquid phase; as a supercage is not large enough to maintain $AlMo_6$ in solution (because of its low solubility, 21.8 mol m^{-3}), these species must be outside the supercages.

Conclusion

This work has tackled the issue of the genesis of zeolite-supported HDS catalysts oxidic precursors prepared from ammonium heptamolybdate incipient wetness impregnation. It appeared that, as in some cases of alumina-supported samples, an Anderson type heteropolyanionic entity $AlMo_6O_{24}H_6^{3-}$ is quantitatively formed. It is preserved during the drying phase. The calcination sees its transformation into a surface aluminum molybdate $Al_2(MoO_4)_3$, probably together with another polymolybdate phase, the location of which is undefined. Upon rehydration of the sample, the Anderson aluminomolybdate anion is partially restored. It has also been shown that, upon impregnation, molybdenum atoms combine with extracted nonframework aluminum atoms to give the Anderson entity. When no extraframework aluminum atom is available to form the Anderson entity, precipitation of ammonium heptamolybdate occurs. Finally, we demonstrated the impossibility for this entity to be present in the supercages of the support.

Acknowledgment. The authors thank C. Méliet for the NMR experiments, F. Villain and V. Briois for the EXAFS experiments, I. Clémençon for the XRD measurements, M. Ledoux for the MoO_3 vapocondensation, and D. Guillaume and S. Lacombe for preparing the zeolite supports.

References and Notes

(1) Payen, E.; Kasztelan, S. *Trends Phys. Chem.* **1994**, *4*, 863.
(2) Stencel, J. M. *Raman Spectroscopy for Catalysis*; Van Nostrand Reinhold: New York, 1990.
(3) Payen, E. *Rev. Inst. Fr. Pet.* **1993**, *48*, 207.
(4) Payen, E.; Grimblot, J.; Kasztelan, S. *J. Phys. Chem.* **1987**, *91*, 6642.
(5) Goncharova, O. I.; Boreskov, G. K.; Yurieva, T. M.; Yurchenko, E. N.; Boldiera, N. N. *React. Kinet. Catal. Lett.* **1981**, *16*, 349.
(6) Spozhakina, A.; Damyanova, S.; Sharkova, V.; Shopov, D.; Yieva, T. *Proceedings of the VIth International Symposium Heterogeneous Catalysis*; Sofia, 1987.
(7) Carrier, X.; Lambert, J.-F.; Che, M. *J. Am. Chem. Soc.* **1997**, *119*, 10137.
(8) Carrier, X.; Lambert, J.-F.; Che, M. *Stud. Surf. Sci. Catal.* **1998**, *121*, 311.
(9) Carrier, X.; Lambert, J.-F.; Che, M. *Stud. Surf. Sci. Catal.* **1998**, *118*, 469.
(10) Carrier, X. Ph.D. Thesis, Université Pierre et Marie Curie, Paris, 1998.
(11) Carrier, X.; Lambert, J.-F.; Che, M. *Stud. Surf. Sci. Catal.* **2000**, *130*, 1049.
(12) Le Bihan, L. Ph.D. Thesis, Université des Sciences et technologies, Lille, 1997.
(13) Le Bihan, L.; Blanchard, P.; Fournier, M.; Grimblot, J.; Payen, E. *J. Chem. Soc., Faraday Trans.* **1998**, *94*, 937.
(14) Bazin, D. C.; Sayers, D. A. *Jpn. J. Appl. Phys.* **1993**, *32*, 249.
(15) Bazin, D. C.; Sayers, D. A.; Rehr, J. J. *J. Phys. Chem. B* **1997**, *101*, 11040.
(16) Revel, R. Ph.D. Thesis, Université de Paris-Sud, Orsay, 1997.
(17) Michalowicz, A. *J. Phys. IV* **1997**, *7*, 235.
(18) Rehr, J. J.; Zabinsky, S. I.; Albers, R. C. *Phys. Rev. Lett.* **1992**, *69*, 3397.
(19) Rehr, J. J.; Mustre de Leon, J.; Zabinsky, S. I.; Albers, R. C. *J. Am. Chem. Soc.* **1991**, *113*, 5135.
(20) Zabinsky, S. I.; Rehr, J. J.; Ankudinov, A.; Albers, R. C.; Eller, M. J. *Phys. Rev. B* **1995**, *52*, 2995.
(21) Ankoudinov, A. L. Ph.D. Thesis, University of Washington, Washington, 1996.
(22) Mariotto, G.; Cazzanelli, E.; Carturan, G.; di Maggio, R.; Scordi, P. *J. Solid State Chem.* **1990**, *86*, 263.
(23) Brunner, E.; Ernst, H.; Freude, D.; Hunger, M.; Pfeifer, H. *Innovation in Zeolite Materials Science*; P. J. Grobet et al., Eds.; Elsevier Science Publishers B. V.: Amsterdam, 1988.
(24) Harrison, W. T. A.; Cheetham, A. K.; Faber, J. *J. Solid State Chem.* **1988**, *76*, 328.
(25) Kunath-Fandrei, G.; Bastow, T. J.; Jaeger, C.; Smith, M. E. *Chem. Phys. Lett.* **1995**, *234*, 431.
(26) Han, O. H.; Lin, C. Y.; Haller, G. L. *Catal. Lett.* **1992**, *14*, 1.
(27) Bare, S. R.; Mitchell, G. E.; Maj, J. J.; Vrieland, G. E.; Gland, J. L. *J. Phys. Chem.* **1993**, *97*, 6048.
(28) Briois, V. *Proceedings of Congrès Galerne 99*, *CNRS*; Piriac sur Mer, 1999.

(29) Hu, H.; Wachs, I. E.; Bare, S. R. *J. Phys. Chem.* **1995**, *99*, 10897.
(30) Bare, S. R. *Langmuir* **1998**, *14*, 1500.
(31) George, G. N.; Cleland Jr., W. E.; Enemark, J. H.; Smith, B. E.; Kipke, C. A.; Roberts, S. A.; Cramer, S. P. *J. Am. Chem. Soc.* **1990**, *112*, 2541.
(32) *ADF Program*, http://www.scm.com.
(33) McKale, A. G. *J. Am. Chem. Soc.* **1988**, *110*, 3763.
(34) Payen, E.; Kasztelan, S.; Grimblot, J.; Bonnelle, J.-P. *J. Raman Spectrosc.* **1986**, *17*, 233.
(35) Gola, A.; Rebours, B.; Milazzo, E.; Lynch, J.; Benazzi, E.; Lacombe, S.; Delevoye, L.; Fernandez, C. *Microporous Mesoporous Mater.* **2000**, *40*, 73.
(36) Menezes, S. M. C.; Camorim, V. L.; Lam, Y. L.; San Gil, R. A. S.; Bailly, A.; Amoureux, J. P. *Appl. Catal. A* **2001**, *207*, 367.
(37) Plazenet, G. Ph.D. Thesis, Université des Sciences et technologies, Lille, 2001.
(38) Boulet-Des Grousilliers, H. Ph.D. Thesis, Université des Sciences et technologies, Lille, 2002.
(39) Borry, R. W., III.; Kim, Y.-H.; Huffsmith, A.; Reimer, J. A.; Iglesia, E. *J. Phys. Chem. B* **1999**, *103*, 5787.
(40) Kim, Y.-H.; Borry, R. W., III.; Iglesia, E. *Microporous Mesoporous Mater.* **2000**, *35*, 495.
(41) Li, W.; Meitzner, G. D.; Borry, R. W., III.; Iglesia, E. *J. Catal.* **2000**, *191*, 373.
(42) Xu, Y.; Shu, Y.; Liu, S.; Huang, J.; Guo, X. *Catal. Lett.* **1995**, *35*, 233.
(43) Fialko, E. F.; Kikhtenko, A. V.; Goncharov, V. B.; Zamaraev, K. I. *J. Phys. Chem. A* **1997**, *101*, 8607.
(44) Tsigdinos, G. A. *Top. Curr. Chem.* **1978**, *76*, 1.